Wave Energy farm assessment in real wave climates
The North Sea

Raghavan, Vaibhav; Alday Gonzalez, Matias; Metrikine, Andrei; Lavidas, George

Important note
To cite this publication, please use the final published version (if applicable).
Please check the document version above.

OMAE2024-120946

WAVE ENERGY FARM ASSESSMENT IN REAL WAVE CLIMATES: THE NORTH SEA

Vaibhav Raghavan[1,*], Matias Alday G.[1], Andrei Metrikine[1], George Lavidas[1]

[1]Delft University of Technology, Delft, Netherlands

ABSTRACT

Wave energy has immense potential and can provide at least twice as much electricity as globally produced now due to its high energy density. Apart from the vast accessibility of the resource, waves are more predictable and available throughout the year when compared to other forms of renewable energies. This makes the development and utilization of wave energy technologies immensely important, in order to meet the renewable energy targets, an example of which is the 40GW by 2050 set as the offshore energy strategy of the European Commission. For wave energy to become a commercially viable power source, individual wave energy converters (WECs) need to be deployed in large numbers similar to what can be seen in the wind industry. Therefore, numerical tools simulating multiple interacting devices becomes highly relevant. This research utilizes the new open-source Boundary Element Method (BEM) based solver HAMS-MREL to analyse the hydrodynamic interactions of mono-array farms of point absorbers inspired by the state-of-the-art Corpower C4 point absorber device in various configurations subjected to waves in different directions. The obtained responses are used to estimate the power absorbed by the arrays in different configurations to obtain the Array Power Matrices, which can be used to study the variability of the q-factors in different sea states and different directions. Furthermore, the obtained Array Power Matrices are used to estimate the power absorbed by the array configurations in the North Sea. This can be a powerful tool for the analysis of the best wave energy farm configurations as it employs a computationally efficient frequency domain-based solver.

Keywords: Boundary Element Method, HAMS-MREL, Wave Energy farms, Frequency domain, Array power matrix

1. INTRODUCTION

The EU has set high targets of 1 GW by 2030 and up to 40 GW by 2050 of ocean energy [1]. In order to achieve the set targets of

the EU, wave energy converters (WECs) need to be deployed in large numbers (farms), leading to lower Levelized Cost of Energy (LCOE). Many WEC devices including the Corpower C4 point absorber device [2], the Mocean Blue X attenuator device [3], AW WaveRoller oscillating surge device [4], amongst others, are on their way to commercial deployment. Therefore, research focused on the study of such devices, particularly in wave farms has become highly relevant. This requires computationally efficient tools that can capture wave-structure hydrodynamic interactions considering multiple bodies.

Many studies have been performed on small to large wave farms in realistic climates particularly with point absorbers. Penalba et.al. [5] focused on wave farms at four locations of the coast of Portugal, Ireland and France with sizes ranging from 5 devices to 39 devices. A frequency domain hydrodynamic model was developed based on BEM (Ansys AQWA) and studies were performed by varying the slenderness (radius/draft) of the device as well as the inter-device distance. It was observed that with increasing number of devices, the lower limit of the q-factor progressively reduced going from 0.95 for 5 WEC farms to 0.68 for the 39 WEC farm. Furthermore, it was observed that with most constructive interactions were observed for large inter-device spacing from $15D$ to $25D$ (D is the diameter of the bouy). Goteman et.al. [6] studied wave farms in Swedish west coast between 64 and 1024 devices with varying geometries using an approximate method, that considers interaction from radiated waves but neglects scattering between bouys. Results showed that with increasing farm sizes keep the inter-device distance constant, the interference was progressively destructive. Bozzi et.al. [7] studied arrays of 4 WECs with varying configurations, inter-device distances ($5D$ to $30D$) and 12 incident wave directions at four locations in the Italian Sea using a time-domain model that couples the hydrodynamic-electromagnetic model with BEM. The arrays were found to be strongly dependent on the incident wave direction and spacing with either too closely spaced or too far leading to destructive interactions. Ideal distances between 10 D and 20 D were reported. The optimal wave farms design lead to a power gain of as much as 3.4 % when comparing with isolated WECs,

---

which were obtained by deriving the array power matrices.

The Corpower point absorber devices are very close to being tested at a farm level within the HiWave-5 project [8] with 3 devices soon to be deployed in addition to currently dry tested Corpower C4 point absorber, off the coast of Agucadoura, northern Portugal. While research in literature has focused on the study of single point absorber devices inspired by the Corpower devices [9–12], there is currently no study that assesses the performance of wave farms employing these devices.

For deployment of wave energy technologies within the EU, utilizing the North Sea could be important. While the resource in the North Sea is lower compared to the West European coast, having a wave climate that is less aggressive is attractive. Furthermore, the North Sea offers a synergy between offshore wind and wave energy, as well as significant infrastructure due to the accelerated development of offshore wind [13]. There is currently very limited research available on wave farms assessments in the North Sea. The work of Beels [14] focused on the optimization and layout of various farm configurations of the Wave Dragon WEC (5 device wave farms) and FO WEC (9 device wave farms) using MILDWave. Results showed that with the Wave Dragon WEC farms in a staggered configuration, the power produced could be as much as 5 times more than a single device when the distance between WECs is $2D_R$ (D_R the distance between the tips of the wave reflectors). With the FO WEC farms, the aligned configuration gave a much better power absorption as compared to the staggered configuration, with power absorption increasing with increased inter-device distance from $3D$ to $5D$. where D is the width of the FO WEC. To the author's knowledge, this is the only study considering the hydrodynamic performance of wave farms in the North Sea.

This work therefore combines the utilization of point absorbers inspired by the state-of-the-art Corpower C4, in various wave farm configurations to assess their performance in realistic wave climates in the North Sea. A frequency domain hydrodynamic model based on BEM is used to analyse the farm to obtain the array power matrices and q-factor matrices, that can be used to effectively assess the performance of the farm in different sea states as well as the overall performance of the wave farm.

2. WAVE DATA

The spectral wave data used in the analysis, is taken from a high resolution hindcast for North Atlantic European waters. This dataset was developed at the Marine Renewable Energies Lab at Delft University of Technology [MREL-Hincast; 15], using a multi-grid implementation of the WAVEWATCH III model [WW3; 16, 17]. The multi-grid 2-way nesting setup considers 3 regular grids with increasing spatial resolution towards European coastal waters: The base grid N_ATL-15M with 0.25° resolution, the first nested grid N_ATL-8M with 0.125° resolution, and the coastal grid EU-2M, with 0.03° of resolution (∼ 2.3 km). The nesting setup is presented in Fig. 1.

In the frequency domain the wave spectrum is discretized in 36 exponentially spaced frequencies from 0.034 to 0.95 Hz, with a 1.1 increment factor from one frequency to the next. In the directional space, 24 directions are used in the base grid N_ATL-15M and 36 directions in N_ATL-8M and EU-2M (resolution of 10°).
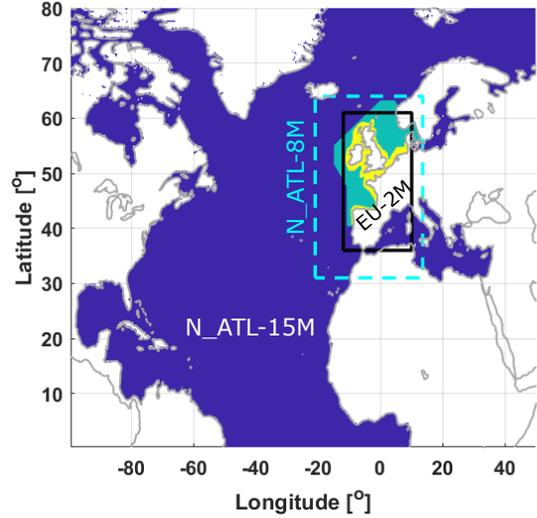
FIGURE 1: Multi-grid setup used in MREL-Hindcast (adjusted from Alday et al. [15]). Active N_ATL-15M grid nodes in dark blue, active nodes from N_ATL-8M grid in green , in yellow active nodes from the high resolution EU-2M grid.

For wave-atmosphere interactions, the ST4 source term package was included [18]. Further adjustments were applied to improve the model performance in the North-East Atlantic starting with the T475 parameterization and following the method from Alday et al. [19]. The Discrete Interaction Approximation [DIA; 20] is used to represent the 4-wave nonlinear interactions. This is a simplified and a computationally "economic" representation of the nonlinear interactions is obtained, which allows to capture the main characteristics of the wave spectrum that are of interest for wave energy applications (e.g.; H_s and T_p).

The model is forced with ERA5 winds [21] for wave generation and included quasi-geostrophic currents (CMEMS product MULTIOBS_GLO_PHY_REP_015_004) to modify the effective wind vector. Ice concentration from Ifremer SSMI-derived product [22] is included to account for wave dissipation at the ice edge in high latitudes. Tidal levels and currents taken from the Atlantic-European North West Shelf-Ocean Physics Reanalysis (CMEMS product NWSHELF_MULTIYEAR_PHY_004_009) to account for stronger wave-current interactions more dominant within the coastal shelf and shallower areas.

The scatter plot for a location considered 42 km off the Dutch coast (Lat 51.999 deg, Long 3.276 deg) is derived from the MREL wave data set. This represents the percentage normalized occurrences of all considered sea states (combination of H_s and T_p), defined as the ratio of the number of occurrences of a specific sea state and the total number of occurrences considered in the thirty year analysis period. This is shown in Fig. 2. This is used later in combination with the power matrices to estimated the power absorbed.

3. HYDRODYNAMIC MODEL OF THE WAVE ENERGY FARM WITH CONVERTER CORPOWER C4 DEVICES

This section briefly describes the hydrodynamic modelling of the wave energy farm consisting of the Corpower C4 wave energy

FIGURE 2: Scatter diagram (Lat 51.999 deg, Long 3.276 deg)
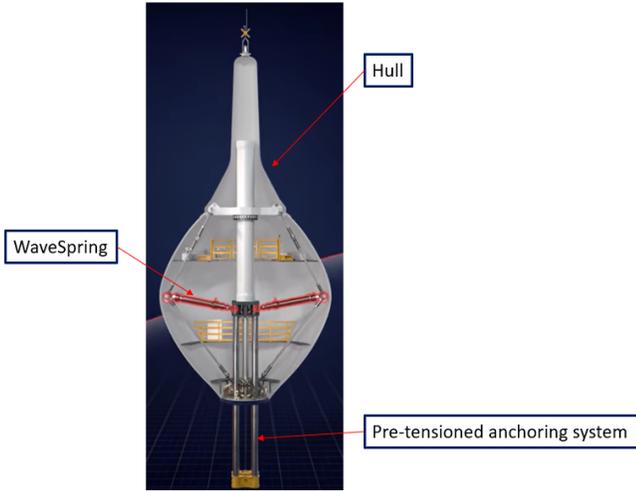
FIGURE 3: Corpower C4 Wave Energy Converter Device [2]

devices. A linearized sub-optimal array power matrix considering viscous losses is derived here, which is used to estimate the power produced at a specific site in the North Sea.

3.1 Device Description

The point absorber device is inspired by the Corpower C4 as shown in Fig. 3. Two interesting features of the device are: 1) Wave-spring system [11] which amplifies the motion and power capture of the device by providing a negative spring function, 2) Pre-tensioning system which replaces some of the mass otherwise needed to balance the buoyancy effect and a composite spherical buoy hull structure, that provides high volume with low mass. The device is anchored to the bottom and employs real-time control algorithms to maximize its power output. The draft of 6 m was assumed by the authors for this study and the natural frequency was calculated based on the aforementioned properties for the single device.

TABLE 1: Properties of the Corpower C4 device

Property	Value	Unit
Diameter	9	m
Height	18	m
Installation depth (minimum)	25	m
Weight	70	tonne
Bouy Draft	6	m
Undamped Natural period (heave)	3	s

3.2 Equations of motion

A frequency domain model was used for estimating the response of the devices in wave farm considering the interactions between them. Only heave motion was considered here. The coupled equations of motion were derived and solved simultaneously. If we consider N devices in the farm, the general equation of motion for the pth device can be given as:

$$[-\omega^2(m_d^{(p)}) + i\omega(b_{PTO}^{(p)} + b_v^p) + c_h^{(p)} + \Sigma_{q=1}^{N}(-\omega^2 m_{33}^{(p)(q)} + i\omega b_{33}^{(p)(q)})]s = f_3^{(p)} \quad (1)$$

where ω is the incident wave frequency, $m_d^{(p)}$ is the mass of the pth device, $b_{PTO}^{(p)}$ is the PTO (Power Take Off) coefficient of the pth device, $b_v^{(p)}$ is the linearized viscous damping coefficient of the pth device, $c_h^{(p)}$ is the hydro-static stiffness coefficient in heaving of the pth device, $f_e^{(p)}$ is the heave exciting force of the pth device, $m_{33}^{(p)(q)}$ and $b_{33}^{(p)(q)}$ are the added mass and radiation damping respectively of the pth device in heave due to the motion of the qth device in heaving. s is the displacement amplitude of the device also referred to as the body excursion. When the amplitude of the incident wave is 1 m, then s represents the RAO (Response amplitude Operator) in heave motion for the device.

Within the scope of this formulation, the following interactions have not been considered - (i) the wave spring component of the device which provides a negative spring stiffness and (ii) the pre-tensioning mechanism (iii) the moorings, as the device is anchored to the seabed directly. The PTO damping is then calculated based on the work of Hals et.al. [23]. For most practical cases, the PTO reactance is negligible or zero and so considering just the PTO damping condition would be sufficient [24]. Furthermore, PTO with reactive control is complex in design, hard to control and expensive which makes passive PTO a preferred option here [25]. Therefore, a sub-optimal passive control has been incorporated within the PTO damping coefficient, based on the formulation which takes into account the losses due to viscosity. To determine the viscous losses, a linearized approach has been used.

3.3 Boundary Element Method (BEM) model

The frequency dependent hydrodynamic coefficients and exciting forces are obtained from the in-house newly developed frequency domain Boundary Element Method (BEM) solver HAMS-MREL (work showcasing its methodology and validation is currently under review in 'Applied Ocean Research'). This solver is built upon the existing open-source BEM solver HAMS
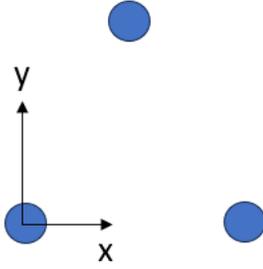
FIGURE 4: Wave farm - Configuration 1

FIGURE 5: Wave farm - Configuration 2

FIGURE 6: Wave farm - Configuration 3

developed by Y.Liu [26]. Shallow water conditions were assumed since the considered depth is 25 m at the location in the North Sea. The mesh taken is from an earlier study done by the authors [27]. Convergence studies were done as part of that. research.

3.4 Overview of the considered cases

Three configurations are considered in this analysis which have different number of devices. These are shown in Fig. 4, Fig. 5 and Fig. 6. The 3 selected configurations are inspired from staggered configurations [7, 28], which have a higher probability of interaction with the incident wave as well as the inter-device interactions that can play an important role in the performance of the wave farm. The interaction within the farm being constructive or destructive will depend on the inter-device spacing and incident wave angle as well. A small inter-device distance of $3D$ (D is the diameter) is selected for this study. This is part of a larger campaign focusing on varying wave resource, incident wave directions, spacings and configurations for WEC arrays.

Two incident wave directions with respect to the positive x-axis are considered for the 3 configurations. Furthermore, 2 cases of PTO control are also considered. The first case is where a constant PTO damping coefficient is considered (for a period of 5 s since around that period the most occurrences are observed in the considered location in the North Sea), and the second case is an optimized PTO damping coefficient per sea state.

This gives a total of 12 cases, that have been shown in Table. 2.

3.5 Natural frequency of the devices in farms

The natural frequency of the devices within a farm configuration were obtained considering all inter-device interactions. The coefficients for both the diagonal and off-diagonal terms in the radiation damping matrix were found to be well below the critical damping of the individual devices considering the Mass and Stiffness (hydrostatic) matrices, and were therefore not considered in the calculation of the natural frequency of the devices. The undamped natural frequencies were thus estimated by an iterative process since the added mass coefficients for all the devices are dependent on the incident wave frequency ω. For every incident wave frequency, the eigen values of the matrix $M^{-1}K$ are obtained, where M is fully populated mass matrix and K is
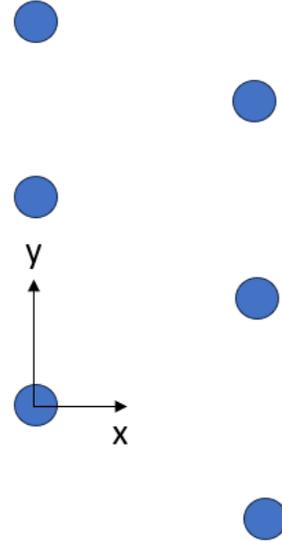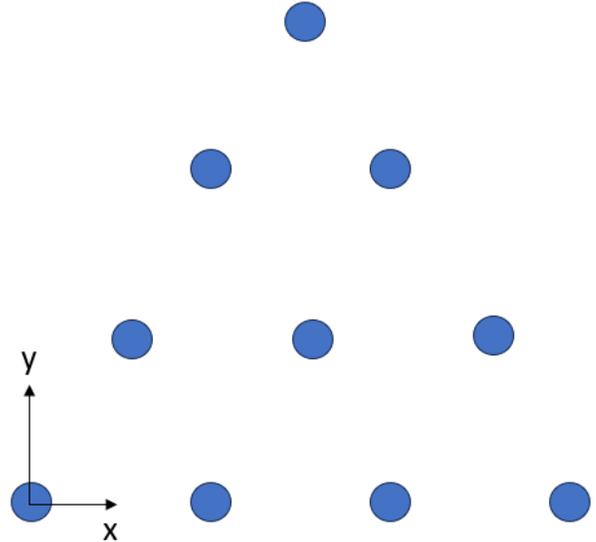
TABLE 2: Overview of the cases considered

Case number	Number of devices	Incident wave direction (degrees)	Control type
1	3	0	Constant PTO coefficient (wave period 5 s)
2	3	45	Constant PTO coefficient (wave period 5 s)
3	3	0	Optimized PTO coefficient for every sea state
4	3	45	Optimized PTO coefficient for every sea state
5	6	0	Constant PTO coefficient (wave period 5 s)
6	6	45	Constant PTO coefficient (wave period 5 s)
7	6	0	Optimized PTO coefficient for every sea state
8	6	45	Optimized PTO coefficient for every sea state
9	10	0	Constant PTO coefficient (wave period 5 s)
10	10	45	Constant PTO coefficient (wave period 5 s)
11	10	0	Optimized PTO coefficient for every sea state
12	10	45	Optimized PTO coefficient for every sea state

the diagonal hydrostatic stiffness matrix. The positive root of the eigen value gives the frequency, which should then be matched with the incident wave frequency to obtain the natural frequency. This process is performed for each device to get its natural frequency which can then be used in the estimation of the linearized viscous losses.

3.6 Sub-optimal passive PTO control and viscous losses

The obtained natural frequency of each device is used to estimate the linearized viscous losses using the Lorentz linearization approach ([29, 30]). The maximum heave displacement of all devices is assumed to be $0.6a$ where a is the radius of the bouy and is applied as a displacement constraint. Sub-optimal passive control including viscous losses was incorporated based on the work of Hals et al. [23] which considers the displacement constraint when obtaining the optimized PTO coefficient. It should be noted that inter-device added mass and radiation damping coefficients (off-diagonal elements of the added mass and radiation damping matrix) are not considered for this calculation. Sub-optimal passive control will henceforth be referred to as sub-optimal control for brevity.

3.7 Power Estimation, Array Power Matrices and q-factor matrices

The average power produced by the WEC over various sea states is quantified in a power matrix. For its computation, irregular wave sea states based on the significant wave height H_s and peak period T_p are considered. From the wave data for the given location, the spectra are derived directly from the MREL dataset per sea state, which can then be used to compute the significant heave amplitude ($\bar{z}_{a_{1/3}}$) and average zero-crossing period (T_{2z}). The methodology is explained in detail in our previous work [27].

When deriving the power matrices, the spectra obtained from the MREL wave data set as well as the JONSWAP spectra is used. For sea states that do not occur at the given location, the JONSWAP spectra is used to derive the average power. For sea states that do occur, the spectra is derived from the MREL dataset. With this procedure, we have a fully populated power matrix that also considers the characteristics of the sea states at the assessment location.

The array power matrices are derived by adding the average power per sea state from all devices in a given farm configuration. This is then compared to the power matrix from a single device to obtain the q-factor matrix. The q-factor for a given sea state (q_{H_s, T_p}) is given in Eqn. 2.

$$q_{H_s, T_p} = \frac{P_{a,farm}(H_s, T_p)}{N \times P_{a,single}(H_s, T_p)} \tag{2}$$

$P_{a,farm}(H_s, T_p)$ is the absorbed power from the farm for a given sea state, and $P_{a,single}(H_s, T_p)$ is from power observed by a single device in isolation in the same sea state. The q-matrix can be used to obtain the sea states when any device within the farm configuration is constructive or destructive. The power matrices and q-matrices are capped to $H_s \leq 9$ m. The total q-factors are calculated by Eqn. 3 can be used as a metric to see if a given farm case is destructive or constructive.

$$q_{total} = \frac{\Sigma_{H_s} \Sigma_{T_p} Scatter(H_s, T_p) P_{a,farm}(H_s, T_p)}{N \times \Sigma_{H_s} \Sigma_{T_p} Scatter(H_s, T_p) P_{a,single}(H_s, T_p)} \tag{3}$$

4. RESULTS AND DISCUSSION

The power matrices for the single devices in isolation can be seen in Fig. 7 and Fig. 8 for the two considered control methods. Array power matrices were derived for all the considered cases (Table. 2), which were then used to obtain the q-factor matrices. For brevity, only the q-factor matrix for Cases 2 and 4 are shown in Fig. 9 and Fig. 10 respectively. The value of the parameter q_{total} is summarized in Table. 3 for all 12 cases. As observed, for all the cases, the interactions within the farm are destructive irrespective of the angle of incidence. All farm configurations perform slightly better when the angle of the incidence wave is at 45 degrees as compared to the 0 degrees incidence. Similar results have been observed in the work of Bozzi et.al. [7] and Penalba et.al. [5], wherein staggered configuration with spacing less than $5D$ and $15D$ respectively (essentially small inter-device spacing) resulted in destructive interference, and thus lower absorbed power in the farm. Furthermore, it is observed that as the number of devices increases within the farm, the interactions become more destructive. This has also been observed in the work

TABLE 3: Total q-factor for all the considered farm cases

Case number	q_{total}[-]
1	0.72
2	0.71
3	0.57
4	0.57
5	0.71
6	0.70
7	0.57
8	0.56
9	0.69
10	0.67
11	0.55
12	0.54

of Goteman et.al. [6], where wave farms of 64 WECs to 1024 WECs showed progressive destructive interference between the devices.

When considering single devices in isolation with sub-optimal constant PTO damping coefficient and sub-optimal damping coefficient per sea state, it is observed the sub-optimal damping coefficient per sea state performs well over a range of sea states. While the single device with constant sub-optimal power coefficient performs well for T_p between 3 and 7s, the single device with sub-optimal damping coefficient per sea state produces more power for T_p between 7 and 20 s, which shows the effectiveness of the optimization strategy adopted. The power matrices reflect this as shown in Fig. 7 and Fig. 8. With farm cases considering the sub-optimal PTO coefficient per sea state, it is observed that the power absorbed is worse than the sub-optimal constant PTO coefficient. This could be attributed to two reasons: 1. When obtaining the optimized PTO coefficient per sea state, the non-diagonal terms in the added mass and radiation damping matrices were not considered. 2. Given that the optimized PTO damping coefficient shifts the performance of the device towards longer wave periods, this could be destructive for a moderate wave resource region such as the North Sea, where most sea states occur at lower peak periods and smaller significant wave heights.

Considering the computational resource (see Table. 4), it can be observed that the time taken is proportional to N_p^2. All the analyses were carried out in a 64 GB node with AMD Rome 7H12 processor (3.3 GHz), with parallelization using 32 cores.

5. CONCLUSIONS

This work explores the performance of wave farm configurations of the soon to be commercialized state-of-the-art point absorber devices, using a frequency domain dynamic model. 3 wave farm configurations (3, 6 and 10 devices) inspired by staggered configurations subject to two incident wave angles (0 and 45 degrees) and two different sub-optimal PTO control methods are compared. The inter-device spacing is taken as $3D$ for all the cases.

Array power matrices are derived for each of the cases, which are used to obtain the q-factor matrices. These indicate which

sea states are constructive or destructive at an array level.

It is observed that for all the farm cases, the interactions are quite destructive in nature giving q_{total} < 1. While all wave farm configurations do slightly better when subjected to an incident wave angle of 45 degrees, with increasing number of devices within the farm, the q_{total} becomes even lower.

Comparing the single isolated devices with the two control methods, it is observed that the sub-optimal PTO damping coefficient per sea state enhances the performance of the device over a wider range of sea states as well as pushes the peak performance to higher wave periods as compared to the constant sub-optimal PTO coefficient (taken at T_p=5s) . However, in the case of the wave farm, the farms with the sub-optimal PTO damping coefficient per sea state performs much worse than the farm with the constant sub-optimal PTO coefficient. This could be due to two reasons: 1. When obtaining the optimized PTO coefficient per sea state, the non-diagonal terms in the added mass and radiation damping matrices were not considered. (Considering these interaction has been effective in earlier studies such as the work of Penalba et.al. [5]) 2. Given that the optimized PTO damping coefficient shifts the performance of the device towards longer wave periods, this could be destructive for a moderate wave resource region such as the North Sea, where most sea states occur at lower peak periods and smaller significant wave heights. Lastly the computational resources were compared for the 3 configurations. It is observed that the time taken is proportional to N_p^2.

The current research will be extended to assess the optimal incident wave directions, spacings and configurations for WEC arrays in combination with optimal PTO control. Furthermore, the performance of WEC arrays with varying wave resource will also be analysed since this is often overlooked.

Using array power matrices and q-factor matrices can be a powerful way of understanding which farm configurations perform well in a certain region, and with powerful open-source BEM tools, this will expedite the deployment of wave arrays.

6. ACKNOWLEDGMENTS

REFERENCES

[1] "North Sea." (2024). URL https://energy.ec.europa.eu/topics/renewable-energy/offshore-renewable-energy_en.

[2] "Corpower." (2024). URL https://corpowerocean.com/wave-energy-technology/.

[3] "Mocean Energy." (2024). URL https://www.mocean.energy/our-technology/.

[4] "AW WaveRoller." (2024). URL https://aw-energy.com/utility-scale-power/.

[5] Penalba, Markel, Touzón, Imanol, Lopez-Mendia, Joseba and Nava, Vincenzo. "A numerical study on the hydrodynamic impact of device slenderness and array size in wave energy farms in realistic wave climates."
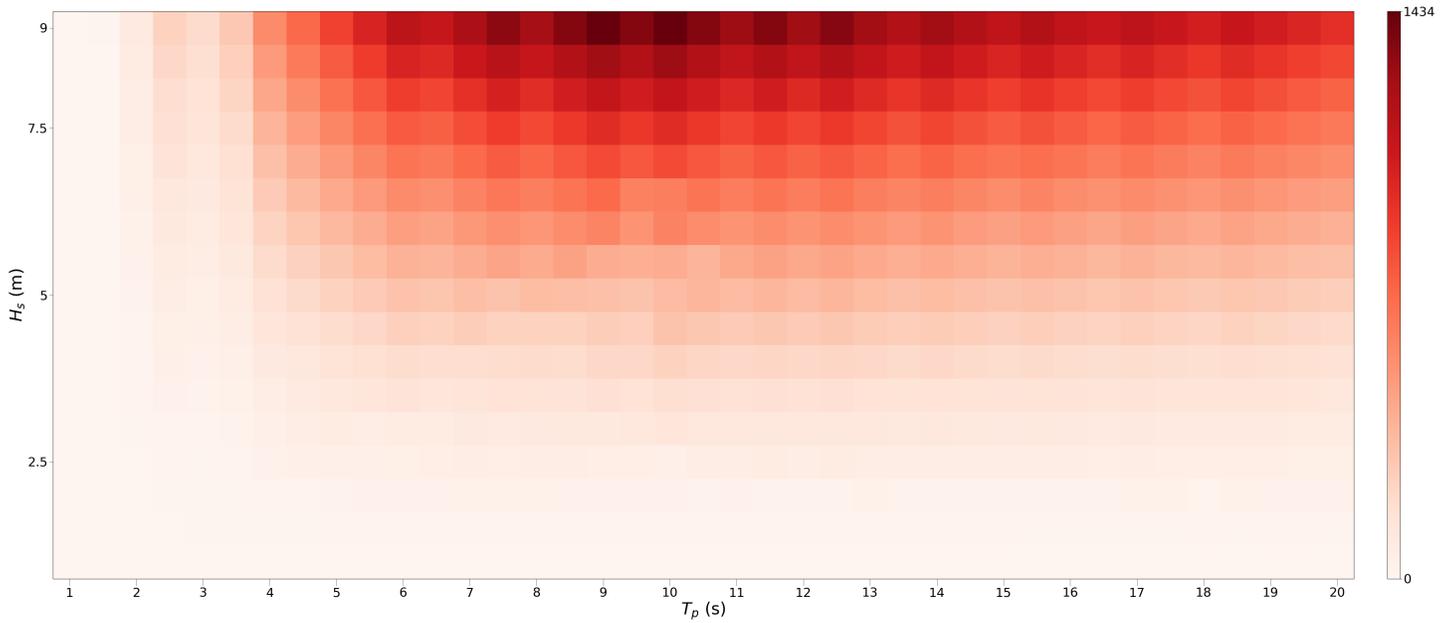
FIGURE 7: Power matrix of a single device with sub-optimal PTO coefficient per sea state (Power in kW)
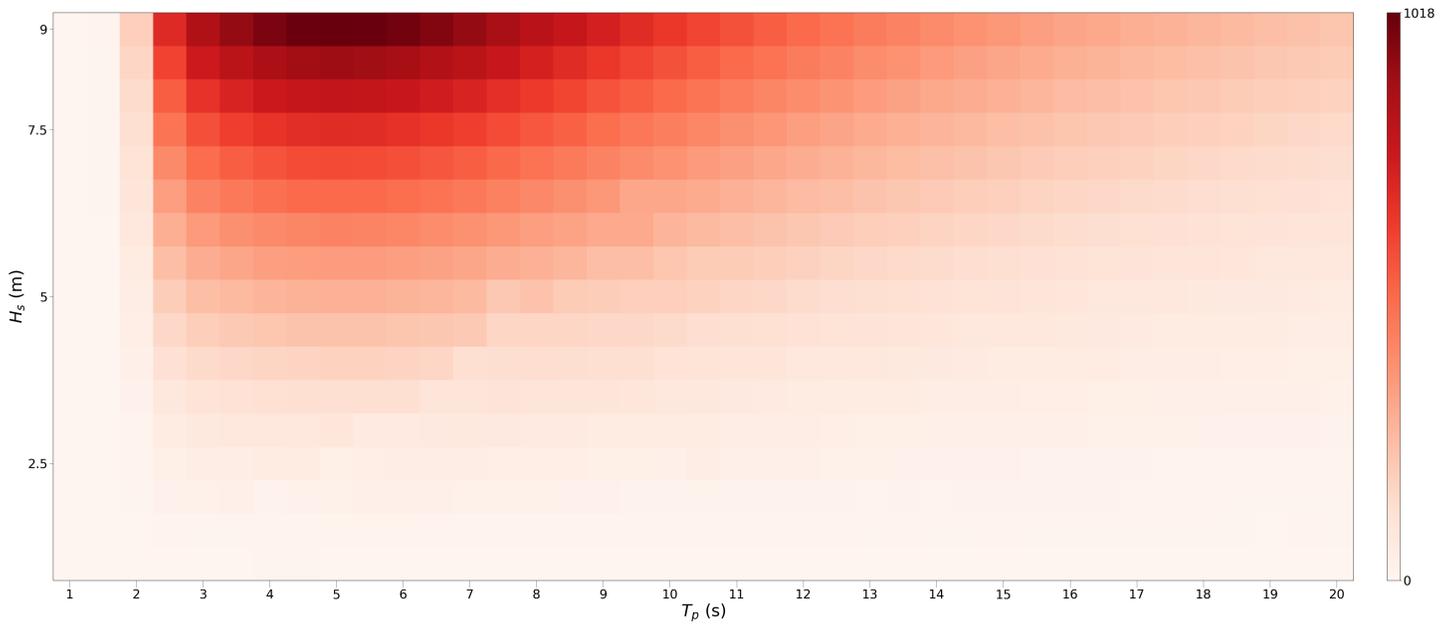
FIGURE 8: Power matrix of a single device with constant sub-optimal PTO at T_p =5s (Power in kW)

TABLE 4: Computational resources utilized by the BEM solver (for both 0 and 45 degrees incident wave angle)

Number of devices	Number of panels (N_p)	Number of frequencies	Computation time (min)
3	4206	40	8
6	8412	40	51
10	14020	40	220

7
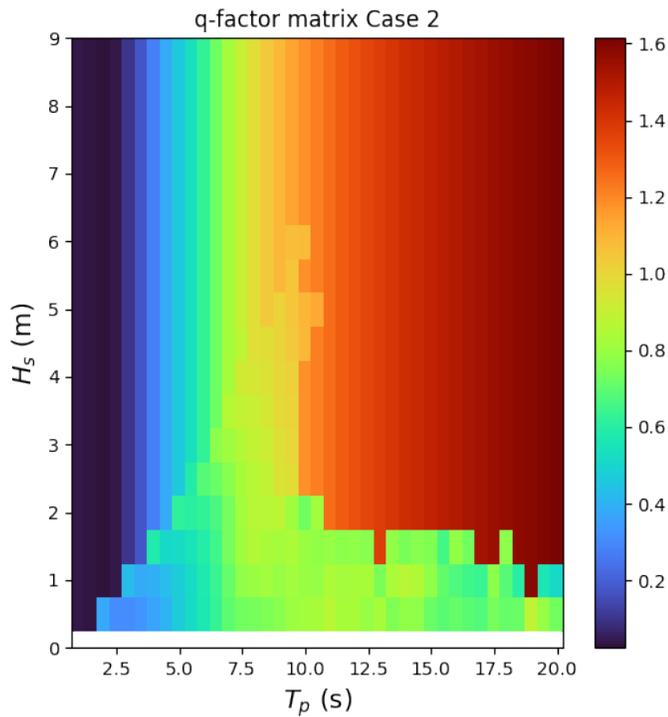
(a) q-factor matrix Case 2
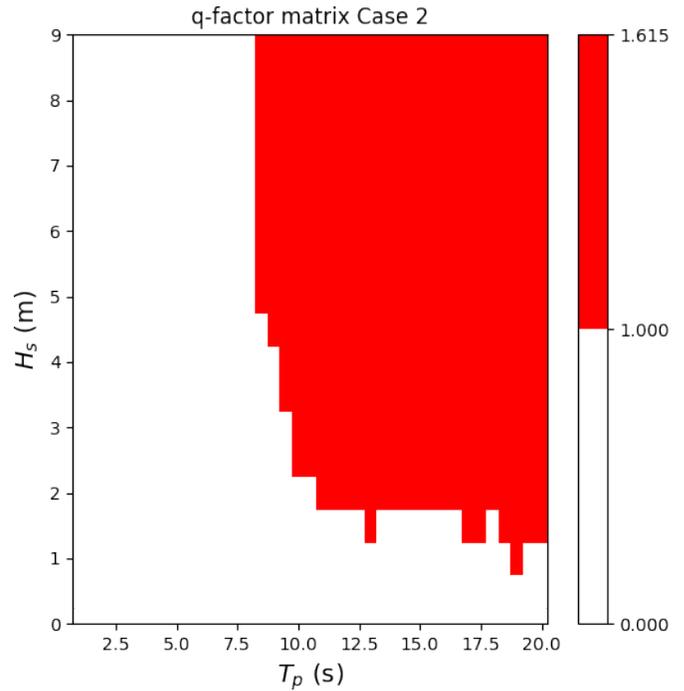
(b) q-factor matrix Case 2 showing constructive and destructive sea states

FIGURE 9: Case 2 q-factor matrix
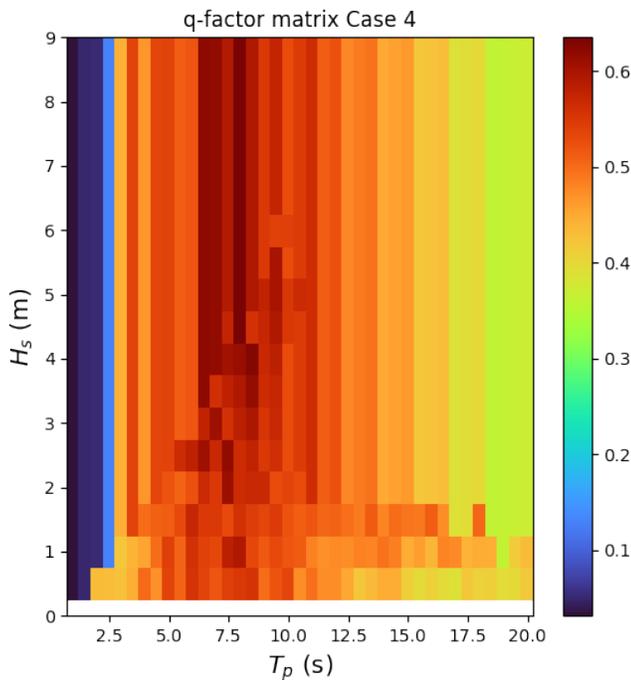
FIGURE 10: q-factor matrix Case 4

Ocean Engineering Vol. 142 (2017): pp. 224–232. DOI https://doi.org/10.1016/j.oceaneng.2017.06.047. URL https://www.sciencedirect.com/science/article/pii/S0029801817303517.

[6] Göteman, Malin, Engström, Jens, Eriksson, Mikael and Isberg, Jan. "Optimizing wave energy parks with over 1000 interacting point-absorbers using an approximate analytical method." *International Journal of Marine Energy* Vol. 10 (2015): pp. 113–126. DOI https://doi.org/10.1016/j.ijome.2015.02.001. URL https://www.sciencedirect.com/science/article/pii/S2214166915000119.

[7] Bozzi, Silvia, Giassi, Marianna, Moreno Miquel, Adrià, Antonini, Alessandro, Bizzozero, Federica, Gruosso, Giambattista, Archetti, Renata and Passoni, Giuseppe. "Wave energy farm design in real wave climates: the Italian offshore." *Energy* Vol. 122 (2017): pp. 378–389. DOI https://doi.org/10.1016/j.energy.2017.01.094. URL https://www.sciencedirect.com/science/article/pii/S0360544217301019.

[8] "Corpower Project HiWave 5." (2024). URL https://corpowerocean.com/projects/.

[9] Giorgi, Giuseppe and Ringwood, John V. "A Compact 6-DoF Nonlinear Wave Energy Device Model for Power Assessment and Control Investigations." *IEEE Transactions on Sustainable Energy* Vol. 10 No. 1 (2019): pp. 119–126. DOI 10.1109/TSTE.2018.2826578.

[10] Wu, Minghao, Wang, Weizhi, Palm, Johannes and Eskilsson, Claes. *CFD Simulation of a Passively Controlled*

Point Absorber Wave Energy Converter. Springer International Publishing, Cham (2018): pp. 499–511. DOI 10.1007/978-3-319-74576-3_34. URL https://doi.org/10.1007/978-3-319-74576-3_34.

[11] Hals, Jorgen, Ásgeirsson, Gunnar Steinn, Hjálmarsson, Eysteinn, Maillet, Jéromine, Möller, Patrik, Guérinel, Matthieu and Lopes, Miguel. "Tank testing of an inherently phase-controlled wave energy converter." *International Journal of Marine Energy* Vol. 15 (2016): pp. 68–84. DOI https://doi.org/10.1016/j.ijome.2016.04.007. URL https://www.sciencedirect.com/science/article/pii/S2214166916300182. Selected Papers from the European Wave and Tidal Energy Conference 2015, Nantes, France.

[12] Ulazia, Alain, Penalba, Markel, Rabanal, Arkaitz, Ibarra-Berastegi, Gabriel, Ringwood, John and Sáenz, Jon. "Historical Evolution of the Wave Resource and Energy Production off the Chilean Coast over the 20th Century." *Energies* Vol. 11 No. 9 (2018). DOI 10.3390/en11092289. URL https://www.mdpi.com/1996-1073/11/9/2289.

[13] Sørensen, H. C. and Chozas, Julia Fernandez. "The Potential for Wave Energy in the North Sea." *3rd International Conference and Exhibition on Ocean Energy (ICOE 2010)*. 2010. ICOE 2010. 3rd International Conference and Exhibition on Ocean Energy ; Conference date: 06-10-2010 Through 08-10-2010.

[14] Beels, Charlotte. "Optimization of the lay-out of a farm of wave energy converters in the North Sea: analysis of wave power resources, wake effects, production and cost." Ph.D. Thesis, Ghent University. 2009.

[15] Alday, Matías, Raghavan, Vaibhav and Lavidas, George. "Analysis of the North Atlantic offshore energy flux from different reanalysis and hindcasts." *Proceedings of the 15th European Wave and Tidal Energy Conference (EWTEC), 3–7 September 2023, Bilbao*. 2023. DOI https://doi.org/10.36688/ewtec-2023-140.

[16] The WAVEWATCH III ® Development Group. "User manual and system documentation of WAVEWATCH III ® version 6.07." Tech. Note 333. NOAA/NWS/NCEP/MMAB, College Park, MD, USA. 2019. 465 pp. + Appendices.

[17] Tolman, H. L. "The numerical model WAVEWATCH: a third generation model for hindcasting of wind waves on tides in shelf seas." Technical Report No. 89-2. Faculty of civil engineering, Delft University of Technology. 1989. ISSN 0169-6548.

[18] Ardhuin, Fabrice, Rogers, Erick, Babanin, Alexander, Filipot, Jean-François, Magne, Rudy, Roland, Aron, van der Westhuysen, Andre, Queffeulou, Pierre, Lefevre, Jean-Michel, Aouf, Lotfi and Collard, Fabrice. "Semi-empirical dissipation source functions for wind-wave models: part I, definition, calibration and validation." *Journal of Physical Oceanography* Vol. 40 No. 9 (2010): pp. 1917–1941. DOI 10.1175/2010JPO4324.1.

[19] Alday, Matias, Accensi, Mickael, Ardhuin, Fabrice and Dodet, Guillaume. "A global wave parameter database for geophysical applications. Part 3: Improved forcing and spectral resolution." *Ocean Modelling* Vol. 166 (2021): p. 101848. DOI https://doi.org/10.1016/j.ocemod.2021.101848.

[20] Hasselmann, S. and Hasselmann, K. "Computation and parameterizations of the nonlinear energy transfer in a gravity-wave spectrum. Part I: a new method for efficient computations of the exact nonlinear transfer." *Journal of Physical Oceanography* Vol. 15 (1985): pp. 1369–1377. DOI 10.1175/1520-0485(1985)015<1369:CAPOTN>2.0.CO;2.

[21] Hersbach, Hans, Bell, Bill, Berrisford, Paul, Hirahara, Shoji, Horányi, András, Muñoz-Sabater, Joaquín, Nicolas, Julien, Peubey, Carole, Radu, Raluca, Schepers, Dinand et al. "The ERA5 global reanalysis." *Quarterly Journal of the Royal Meteorological Society* Vol. 146 No. 730 (2020): pp. 1999–2049. DOI 10.1002/qj.3803.

[22] Girard-Ardhuin, F. and Ezraty, R. "Enhanced Arctic sea ice drift estimation merging radiometer and scatterometer data." *IEEE Transactions on Geoscience and Remote Sensing* Vol. 50 (2012): pp. 2639–2648. DOI 10.1109/TGRS.2012.2184124.

[23] Hals, Jorgen, Bjarte-Larsson, Torkel and Falnes, Johannes. "Optimum Reactive Control and Control by Latching of a Wave-Absorbing Semisubmerged Heaving Sphere." Vol. 21st International Conference on Offshore Mechanics and Arctic Engineering, Volume 4 (2002): pp. 415–423. DOI 10.1115/OMAE2002-28172. URL https://asmedigitalcollection.asme.org/OMAE/proceedings-pdf/OMAE2002/36142/415/4545242/415_1.pdf, URL https://doi.org/10.1115/OMAE2002-28172.

[24] Alves, M. "Chapter 2 - Frequency-Domain Models." Folley, Matt (ed.). *Numerical Modelling of Wave Energy Converters*. Academic Press (2016): pp. 11–30. DOI https://doi.org/10.1016/B978-0-12-803210-7.00002-5. URL https://www.sciencedirect.com/science/article/pii/B9780128032107000025.

[25] Zou, Shangyan, Abdelkhalik, Ossama, Robinett, Rush, Bacelli, Giorgio and Wilson, David. "Optimal control of wave energy converters." *Renewable Energy* Vol. 103 (2017): pp. 217–225. DOI https://doi.org/10.1016/j.renene.2016.11.036. URL https://www.sciencedirect.com/science/article/pii/S0960148116310059.

[26] Liu, Yingyi. "HAMS: A Frequency-Domain Preprocessor for Wave-Structure Interactions—Theory, Development, and Application." *Journal of Marine Science and Engineering* Vol. 7 No. 3 (2019). DOI 10.3390/jmse7030081. URL https://www.mdpi.com/2077-1312/7/3/81.

[27] Alday, Matias, Raghavan, Vaibhav and Lavidas, George. "Analysis of the North Atlantic offshore energy flux from different reanalysis and hindcasts." *Proceedings of the European Wave and Tidal Energy Conference* Vol. 15 (2023). DOI 10.36688/ewtec-2023-140. URL https://submissions.ewtec.org/proc-ewtec/article/view/140.

[28] Battisti, Beatrice, Giorgi, Giuseppe and Fernandez, Gael Verao. "Balancing power production and coastal protection: A bi-objective analysis of Wave Energy Converters." *Renewable Energy* Vol. 220 (2024): p. 119702. DOI https://doi.org/10.1016/j.renene.2023.119702. URL https://www.sciencedirect.com/science/article/pii/S0960148123016178.

[29] Malta, Edgard B., Gonçalves, Rodolfo T., Matsumoto, Fabio T., Pereira, Felipe R., Fujarra, André´ L. C. and Nishimoto, Kazuo. "Damping Coefficient Analyses for Floating Offshore Structures." Vol. 29th International Conference on Ocean, Offshore and Arctic Engineering: Volume 1 (2010): pp. 83–89. URL https://asmedigitalcollection.asme.org/OMAE/proceedings-pdf/OMAE2010/49095/83/4590385/83_1.pdf, URL https://doi.org/10.1115/OMAE2010-20093.

[30] Folley, M. and Whittaker, T. "Spectral modelling of wave energy converters." *Coastal Engineering* Vol. 57 No. 10 (2010): pp. 892–897. DOI https://doi.org/10.1016/j.coastaleng.2010.05.007. URL https://www.sciencedirect.com/science/article/pii/S0378383910000700.